A Summary of Test Results from a NASA Lift + Cruise eVTOL Crash Test

Justin Littell
Justin.D.Littell@nasa.gov
Research Aerospace Engineer
NASA Langley Research Center
Hampton VA, 23681

Jacob Putnam
Jacob.B.Putnam@nasa.gov
Research Aerospace Engineer
NASA Langley Research Center
Hampton VA, 23681

ABSTRACT

On November 9, 2022, the National Aeronautics and Space Administration (NASA) conducted a full-scale crash test of the NASA Lift+Cruise (LPC) reference vehicle at the NASA Langley Research Center (LaRC) Landing and Impact Research Facility (LandIR) under combined vertical and horizontal impact conditions to simulate a severe but survivable crash. The LPC test article is a carbon-composite skin/frame structure design, developed and fabricated for the cabin section only. The test utilized various configurations of seats and Anthropomorphic Test Devices (ATDs, a.k.a. crash test dummies) intended to encompass a variety of occupant conditions. In addition, an in-house developed energy absorbing subfloor was utilized for the evaluation of load attenuation. The overhead mass was simulated using attached lifting hardware and other systems were simulated using ballast mass.

The test article impacted the ground with velocities of 38.1 ft/s horizontal and 31.4 ft/s vertical. During the first approximately 38 milliseconds (ms), the cabin section experienced a large amount of acceleration on the belly which was attenuated by the subfloor structures and seats. Over the next approximately 160 ms, the test article experienced failure in the a-, b- and c-pillars, leading to a partial collapse of the overhead structure. Test data was collected on the belly, floors, seats, overhead mass, and tail. In addition, there was high speed full-field digital image correlation analysis data collected on the port side skin surface. Collected ATD data showed that the ATDs seated in the energy absorbing seats experienced lumbar loads below regulatory limits. Even without an energy absorbing seat, the energy absorbing subfloors crushed as intended, and limited the load on the large 95th percentile ATD to 10% over suggested limits. The collapse of the roof did affect the 95th percentile ATD, which showed high neck loading values due to head contact. While the energy absorbing subfloor and energy absorbing seats both contributed to occupant load attenuation, further optimization is suggested to increase their robustness.

INTRODUCTION

The emergence of the electric Vertical Take-off and Landing (eVTOL) industry represents a great opportunity to change the paradigm of air travel by developing vehicles and systems that allow for increased mobility in urban environments with increased efficiency. The eVTOL industry is represented by a variety of aircraft manufacturers, city planners, government, academia, and other interested parties working toward future widespread implementation. NASA has been focused on conducting research for future eVTOL vehicles through various areas including noise [1], aerodynamics [2], and human factors [3].

A team at NASA Langley Research Center (LaRC) has been conducting investigations into the crashworthiness of eVTOL vehicles undergoing events such as hard landings or crashes. The focus areas include energy absorbing mechanism development and characterization of occupant loading conditions and vehicle performance under emergency and crash type conditions. As a part of this research, NASA proposed developing a reference eVTOL test article and conducting a full-scale drop test.

After preliminary impact analyses were conducted of a quadrotor eVTOL vehicle [4], the NASA Lift+Cruise (LPC) vehicle was selected as the test article for demonstration. The LPC vehicle design was developed as a NASA concept vehicle [5] and

Presented at the Vertical Flight Society's 79th Annual Forum & Technology Display, West Palm Beach, FL, USA, May 16-18, 2023.

represents a six seat, high-wing design intended to take off and land vertically while operating like an aircraft during cruise. The LPC test was conducted to achieve four objectives: to acquire data on a representative eVTOL vehicle structure to inform industry consensus standards development, to validate computer simulation models, to generate data on advanced Anthropomorphic Test Devices (ATDs) for the evaluation of injury, and to test energy absorbing systems for the subfloors and seats in a full-scale environment.

TEST ARTICLE DEVELOPMENT

Due to their main expected contribution to crashworthiness and occupant load, the section of the LPC vehicle chosen for fabrication included all primary structure from the nose to the aft bulkhead. The test article consisted only of the primary structure that was assumed to a role on the occupant response, and effort was primarily spent preparing these sections for test.

While the outer mold line (OML) was based on the LPC design, the internal support structure was primarily developed through the use of computational simulations [6]. The sizing and spacing of the internal stiffeners, material layup stacking sequence and other parameters were baselined from conventional practices and verified and modified using computational simulations. Analyses ensured that the section would withstand inertial loads found in 14 CFR 27.561 [7], which was one of the main design factors used in determining sizing.

The skin and frame components were composed of layers of 3k-70-PW carbon fabric infused with INF-114 room temperature cure Epoxy resin, and vacuum bagged using large molds. The skin was built in four sections and assembled with post-cure bond lines on the top, belly, port, and starboard centerlines of the structure. The skin and frame stiffeners were composed of six and eight layers, respectively, and in a [0°/45°] repeating layup. There was no keel beam and no lateral subfloor shear webs. The subfloor energy absorbing concepts were fabricated and integrated during the test buildup to act as load paths within the subfloor structure. An illustration of the LPC test article main structure is shown in Figure 1.

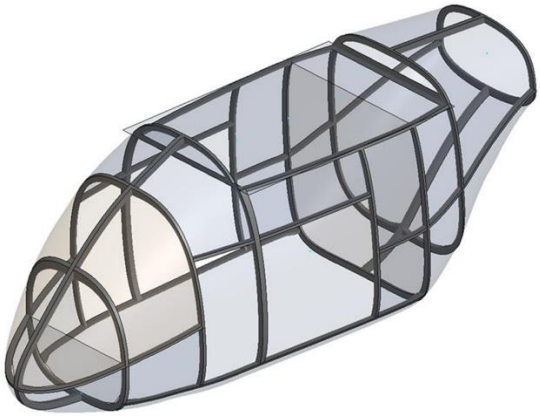

Figure 1 - Structural components of the LPC test article.

The main cabin frame sections were longitudinally spaced approximately every 24 inches until the rear bulkhead, with the exception of the large openings representing the doors on the test article. There were two additional frame sections behind the rear bulkhead. One was located during the cabin to tail transition and a final frame was positioned at the tail rear opening.

A windscreen was developed from 0.125-inch acrylic sheet and was intended to provide additional structural rigidity. The doors were not added to the structure as they were thought to not add structural rigidity. A picture of the empty as-built LPC cabin section, prior to test build-up, is shown in Figure 2.

Figure 2 - Empty Lift + Cruise section.

The section did not include a nose component, nor any subfloor structure. A nose was originally a variable intended to be designed and fabricated to various geometries to study the effects of scooping and plowing for some expected test cases. The actual nose used for the test was a rounded design that was more blunt than the original LPC geometry.

The energy absorbing (EA) subfloor concepts used were of a modular type and intended to represent a crushable structure under each individual seat rather than a beam/frame system which would be utilized for the entire cabin section. The original intent was to develop optimized EAs under each seat/ATD configuration; however, it was later decided that because there was no subfloor keel beam, longitudinal stability must be provided by continuous seat rails and the seat rails would not be sectioned into smaller pieces for each individual energy absorbing component. The drawback of keeping the seat rails as one long continuous beam was possible load path transfer from one seat position to the others. Therefore, EAs were not optimized to individual occupant weights.

The development of the EA concepts began in 2020 and have continued to evolve through a series of tests documented in [8-9]. The EAs were a modular design, each comprised of a cruciform section with added longitudinal bracing, which made them resemble an enclosed cross. The sections were fabricated out of hybrid carbon/Aramid plain weave fabric oriented at 45 degrees, vacuum bag and cured at room temperature with Epon 828 resin. Four-layer cruciform subfloors were positioned directly under each seat, while five-layer configurations were placed under the data acquisition systems, which were also located on the floor in between the rows of seats. In all, there were nine cruciforms present for the test. Each cruciform was riveted to the belly of the airframe through a bottom flange, while the top was notched, bent, and glued to the floor sections. The six aft cruciforms are shown in Figure 3.

Figure 3 - Energy absorbing subfloor components.

The floors were a sandwich composite composed with four layers of carbon fiber face sheets and a closed cell rigid polyurethane foam core cured using a room temperature cure resin. Tests were conducted to represent the bending stiffness of an aircraft cabin floor and were performed to ensure that floors were representative of a composite floor design. The floors were fabricated in two-foot lengths and meant to sit above a single row of the modular EA subfloors. A composite floor, shown under vacuum bag during fabrication, is shown in Figure 4.

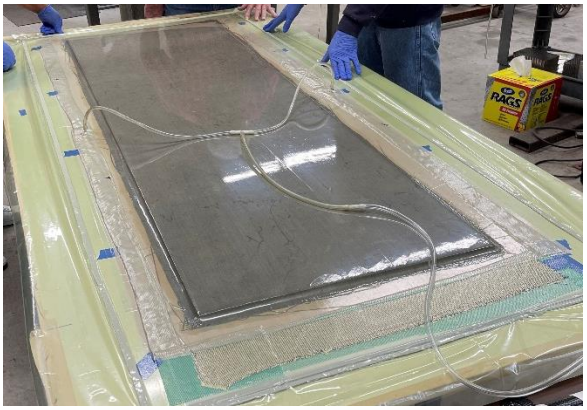

Figure 4 - Composite floor fabrication.

Six ATDs were utilized on the test seated in a combination of energy absorbing and rigid seats. The test configuration is shown in Figure 5, noting that forward is to the left. The ATD sizes ranged from a small 10-year-old (YO) sized Hybrid III (HIII) to a large 95th percentile HIII. There were three 50th percentile ATDs, two of which were HIII's utilizing the straight spine configuration, labeled "FAA", while the third was a Hybrid II (HII) build.

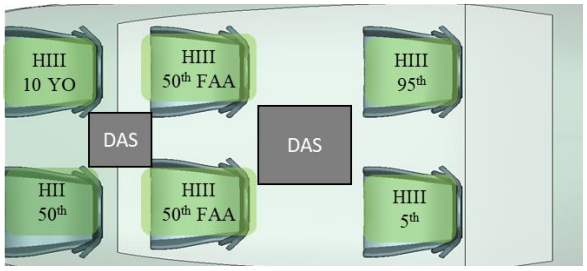

Figure 5 - ATD configuration for test (forward on left).

The design for NASA energy absorbing seat was first proposed in [8] and analyzed in [4]. The EA design itself is of a tube with accordion shaped walls designed to fold and crush in a stable and predictable manner.

In order to implement the design into the test, hardware was built to accommodate two of the accordion shaped EAs integrated into the front seat legs. The rear seat legs provided support, but mainly acted as guides for the rear portion for the seat to follow during the crush. Brackets attached to the seat back were allowed to travel along the rear tubes allowing the seat to freely crush on the front EAs. The EAs were oriented at a nominal 10-degree angle to the vertical based on predictions of the expected forward loads. A composite seat bucket was used for the seat itself, and an aircraft certified three-point harness was used as the restraint. The NASA developed energy absorbing seat is shown in Figure 6.

Figure 6 - NASA developed EA seat.

The other rigid seats were also designed and assembled in-house at NASA LaRC. Two of the three other rigid seats utilized carbon fiber seat buckets, while the rigid seat for the HIII 10 YO was an aluminum bucket. All rigid seats utilized rigid aluminum seat legs and attached directly into the seat track. All rigid seats utilized aircraft certified three-point harnesses. The rigid composite seat design is shown in Figure 7.

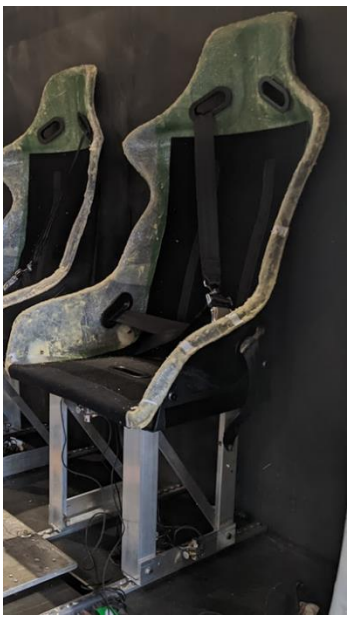

Figure 7 - Composite rigid seat design.

The overhead mass was the final major component added to the test article. The overhead mass was designed based on assumptions pertaining to the overhead wing configuration. Early LPC models included wing representations with a rigid wingbox to examine the effects of the wings on the vehicle structure [6]. However, the wings could create unnecessary hazards because of possible interference with the lifting equipment, so the decision was made early in the test development to test without them. By removing wing structure for the test and replacing with a concentrated mass over the cabin section, the entirety of the overhead wing weight including motors, rotors, batteries, and the structure itself were positioned as a mass concentrated over the cabin section.

In addition, since the LPC test article was not built with attachment fittings to interface with the necessary cabling needed to lift and swing the test article during the test, the overhead mass was outfitted with lifting interfaces. The overhead mass was designed to conform to the wingbox opening in the top of the test article and built using welded steel box beams with lifting lugs. The entire weight of the overhead structure was 1,080 lb. and is shown in Figure 8.

Figure 8 - LPC lifting hardware.

The tail mass was simulated with 500 lb. of ballast attached directly to the tail opening and based on the weight of the tail components in the LPC design. Additional items such as avionics, wiring, environmental controls and others were not added to the test article because it was assumed these added components would not be affect the performance of the primary structure or contribute to the occupant response.

The final weight of the test article including all additions was 3,450 lb. The longitudinal center of gravity (CG) was at station 127.5 and vertical CG was approximately 48 inches above the belly. The port side of the test article was painted in a stochastic black and white speckle pattern to generate data on surface deformations through digital image correlation methods, and tracking markers were placed on areas of specific interest in order to generate discrete tracking data. The final, pre-test configuration of the LPC test article is shown in Figure 9 with the CG location represented by the yellow circle located near the aft and top of the opening.

Figure 9 - Pre-test configuration for LPC test article.

Preliminary simulations on the LPC vehicle were performed to help guide the impact conditions. Existing regulations [10-11] were consulted and other full-scale test data examined [12]. The impact conditions targeted were approximately 25 ft/s to 30 ft/s in the vertical direction and approximately 40 ft/s in the horizontal.

Onboard data systems recorded the test article response at a variety of locations. The data system components were split into two small pallets which were mounted onto the floor between the first and second rows and again between the second and third rows of seats. The data system recorded 128 channels of data at a sampling rate of 20 kHz. Accelerometers were placed on the belly between the first and second rows, on the floors at the a-pillars, rear bulkhead and all seat bases and pans. Additional accelerometers were placed on the lifting hardware and tail. Additional sensors included a timecode signal and four lifting cable load cells. Five out of the six ATDs also interfaced with the onboard data systems. The remaining ATD contained its own internal data system, which was separately triggered and recorded. All ATD instrumentation included pelvic, chest, and head accelerations and lumbar loads and moments. For all of the HIII ATDs, neck loads were also collected along with head rotational rate. In all, a total of 164 channels of data were collected from the test.

High speed cameras were also present for the test. Cameras imaged the test from all sides and recorded at a minimum of 1 kHz using 1-megapixel sensors. The main digital image correlation cameras recorded monochrome at a resolution of 4 megapixels.

RESULTS

The test was conducted on November 9, 2022. The test article impacted the ground with velocities of 38.1 ft/s horizontal and 31.4 ft/s vertical at a 0.6-degree nose down pitch and an approximate 2-degree yaw. A test image sequence taken from the port side is shown in Figure 10 using visual indicators captured from notable events.

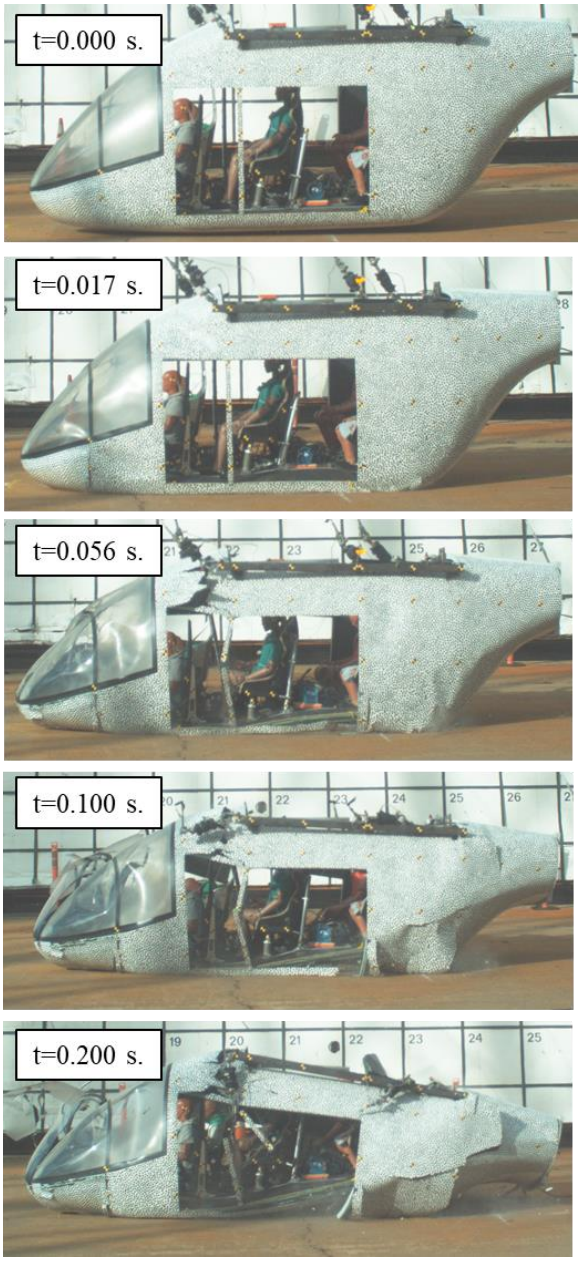

Figure 10 - Test image sequence.

The sequence in Figure 10 shows five notable times during the impact event. The top image depicts the test article just as it has contacted ground at t=0 s. Immediately after impact, the EA components in the subfloors began to stroke. The upper middle image in Figure 10 shows the time in which the NASA EA seat stroke began to occur, which was approximately 17 milliseconds (ms) after initial ground contact. During this time, the overhead mass compressed the test article frame stiffeners, however there were no failures visible. The middle image depicts the test article at 56 ms after impact, which was the time of maximum stroke on the NASA EA seat. There were visible failures located in the forward cabin area. While not depicted in the image sequence, the first visible signs of failure in the vertical frame stiffeners began to occur approximately 36 ms after impact.

The fourth picture in Figure 10 shows the test article at 100 ms after impact where the b- and c-pillars have failed leading to the overhead mass to sink further. However, because the frame section around the nose on the port side had not failed, the mass began to tilt at an upward angle. The further compression of the aft end of the mass continued for the next 100 ms, until approximately 200 ms after the impact. Shortly after 200 ms post-impact, the overhead mass reached its maximum crush depth, and vertical motion of the overhead mass stopped. However, the test article continued to slide out for 2.4 seconds. The test article came to rest in its post-test configuration approximately 2.65 seconds after initial impact. Post-test inspections of the test article started immediately after the test article had come to rest. The port side damage is first shown in Figure 11.

Figure 11 - Post-test damage in the port side.

Post-test inspections of the port side of the test article revealed both the b- and -c pillar failures leading to the overhead collapse. The frame section in the nose was largely undamaged which allowed for the forward portion of the cabin to retain its internal volume.

A post-test photo of the nose section is next shown in Figure 12.

Figure 12 - Post-test damage in the nose section.

As shown in Figure 12, large amounts of damage and failures occurred in the nose portion of the test article. The forwardmost frame section broke away from the center longitudinal stiffener on the starboard side, shattering the starboard windscreen. The additional lower frame section on the starboard side also began to separate from the nose, but was still attached in the center of the nose, restraining it from breaking apart entirely. The starboard side is next shown in Figure 13.

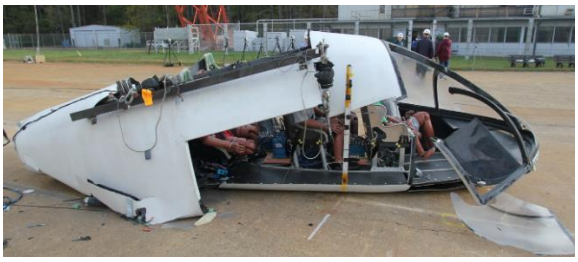

Figure 13 - Post-test damage in the starboard side.

Post-test inspections of the starboard side of the test article revealed both the a-, b- and -c pillar failures leading to the overhead collapse. Since the a-pillar collapsed on the starboard side, the roof vertical motion was higher than that on the port side. Finally, the floor structure was examined. The port side floor for the second and third row of seats is shown next in Figure 14.

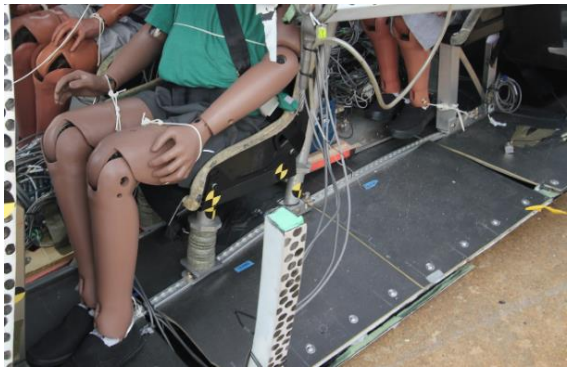

Figure 14 - Port side floor for second and third row.

There was a large amount of warpage on the floor and seat tracks, which was due to the compression of the subfloor EA structures. However, the floors stayed attached to the longitudinal stiffeners on both sides of the test article and the seat tracks remained attached to the floor, indicating the stiffness was sufficient to ensure that the EA structures would be able to produce the intended crush forces and be utilized as intended. Note the failed b-pillar column is visible in the foreground of Figure 14.

Accelerations were acquired at various locations around the test article. All accelerations were filtered in accordance with SAE-J211 [13]. Comparisons to additional filter values are also provided in order to study the structural loads within the test article. Starting with the airframe floor/frame junction data, the starboard side experienced periodic data dropout leading to anomalous data at particular times, so the port side data is presented instead. The underlying data filtered in accordance with SAE J211 still showed significant oscillations, so additional low-pass filtering was used to determine the underlying pulse shape at the floor. Acceleration on the airframe on the belly and at the floor level is shown in Figure 15.

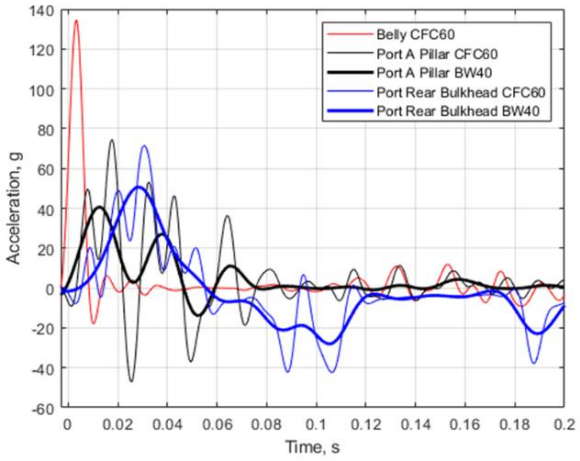

Figure 15 - Port side floor level acceleration.

Using the SAE J211 filtering criteria, the peak airframe belly accelerations were 135 g, which only occurred for a duration of 8 ms. This short duration pulse represented a shock load on the test article at first contact with the ground and is not representative of the load imparted to the occupant compartment. When examining the floor accelerations, the belly impact was attenuated primarily through the airframe deformation and the overall subfloor crushing. When examining the SAE J211 filtered data for the port side frames, the accelerations indicated peak values of 74.3 g and 71.1 g for the a-pillar and rear bulkhead, respectively. However, there were significant oscillations present, due to the compliance of the test article, so additional filtering of a Butterworth (BW) 4-pole 40 Hz lowpass filter was applied. With the oscillations removed, the peak accelerations reached 40.6 g for the forward a-pillar, and 50.7 g for the rear bulkhead. Both pulses were triangular in shape and lasted for approximately 60 ms for the a-pillar location and 55 ms for the rear bulkhead. These times were generally in line with the time needed for EA crushing, appearing slightly longer since the measurements were not directly over the EA components.

Next, the horizontal accelerations at the belly location are plotted and shown in Figure 16.

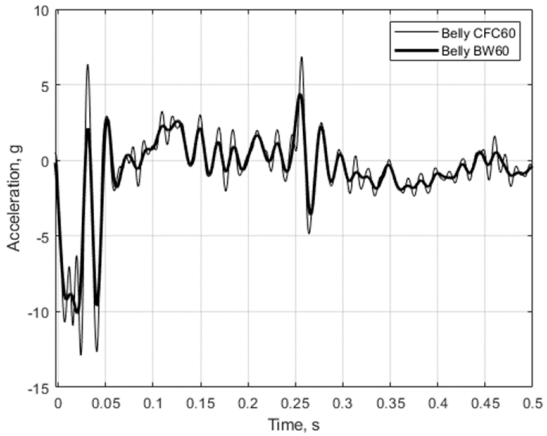

Figure 16 - Airframe horizontal acceleration.

The horizontal accelerations filtered in accordance with SAE J211 also showed oscillations similar to the vertical direction, so an additional lower BW 60Hz lowpass filter was used. The acceleration response with the highest magnitudes occurred for approximately the first 50 ms after impact. The acceleration pulse resembled a trapezoid in shape with peak values less than 10 g for the 60 Hz filter. Integrating the belly acceleration for the first 50 ms after impact produced a velocity delta of 9.7 ft/s. After this first 50 ms, there was no significant acceleration recorded prior to the test article coming to rest. It took an additional 2.635 seconds after the initial acceleration for the test article to come rest, leading to an average acceleration value of 0.4 g in the late time history of the post-test response. The relatively low friction between the concrete surface and the test article belly allowed for this large slide out distance to occur.

Next, accelerations on the overhead mass were examined. The vertical acceleration for the aft starboard side is shown in Figure 17.

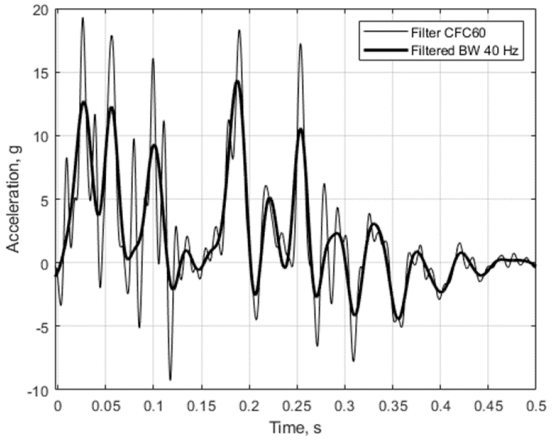

Figure 17 - Aft starboard side overhead mass acceleration.

Both the CFC60 filter and the lower BW40 filters did not change the underlying pulse shape in the overhead mass location, however the lower BW40 did change magnitudes. The overhead mass experienced two main pulses during the test. The first occurred during the first 100 ms and showed sustained positive acceleration values (when examining the BW40 curve) that occurred during the time of support frame section compression and failure. There is a second group of spikes that occurred starting at approximately 166 ms and lasting until 265 ms. This acceleration did not appear to be sustained at a positive value, but rather the effect of potentially two discrete events which occurred at 188 ms and 253 ms. It cannot be determined what caused the first spike, however an accelerometer located on the tail points to evidence that the second spike was a result of the tail strike. There were no other significant events to take place after the tail strike occurred. Additional evidence is captured from the video which showed after this time the major crushing has occurred and the vehicle experienced only post-impact slide-out. The tail vertical acceleration was next examined and is shown in Figure 18.

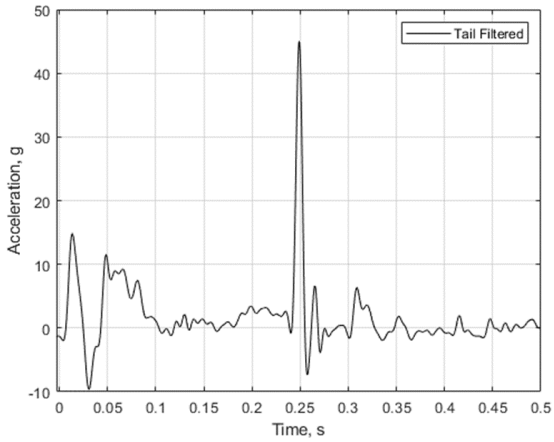

Figure 18 - Tail acceleration.

The tail accelerations indicted an initial spike of approximately 14.8 g before shifting to a -9.5 g during the first 30 ms after impact. However, after this initial oscillation, the tail experienced sustained acceleration of less than 10 g for the next 50 ms, which was caused by the roof collapse event happening during this time. The large spike occurring approximately 250 ms after impact was when the tail strike onto the impact surface occurred.

Next, the various occupant loads that were collected during the test were evaluated. The data acquired from the test was evaluated using several established metrics including the Head Injury Criteria (HIC) [14], Neck Injury Criteria (Nij) [14] and Lumbar Load criteria.

The first metric used for evaluation of occupant loading is the Head Injury Criteria. This metric is based on the following equation:

$$HIC = max\left\{\left[\frac{1}{t_2-t_1}\int_{t_1}^{t_2} a(t)dt\right]^{2.5} * (t_2 - t_1)\right\} \quad (1)$$

The input acceleration is the root sum squared of the head acceleration time history. This time history enters into equation 1, which produces a single value for each calculation, which is then evaluated using a sliding time window. The Federal Aviation Administration (FAA) requires a HIC metric value of less than 1,000 for both general aviation [10] and rotorcraft [11], indicating that a window of 36 ms is used in evaluation. This HIC metric is often known as "HIC36".

All HIC36 values for the adult sized ATDs (5th, 50th) were under the established limits of 1,000. However, two ATDs experienced partial data drop out so the calculation was unable to be performed. The 95th ATD experienced signal loss in the vertical direction while the 50th HII ATD experienced signal loss in the horizontal direction. Additionally, HIC values were not calculated in the 10YO ATD due to no established metrics available to compare the data. The summary of the HIC36 values is shown in Table 1.

Table 1 - ATD HIC values.

ATD	HIC36 Value
1 – HIII 10 YO - Front Stbd	Not Calculated
2 – HII 50th - Font Port	Not Available
3 – FAA HIII 50th - Middle Stbd	140
4 – FAA HIII 50th - Middle Port	98
5 – HIII 95th - Rear Stbd	Not Available
6 – HIII 5th - Rear Port	202

The obtained HIC values are well below the 1,000 threshold, with the maximum of 202 which occurred in the rear 5th ATD. A large value or large spike would be indicative of the head impacting an object during the test. As such, no head-strike was identified in the three ATD's for which HIC was calculated.

Next, Nij values were next examined for all adult ATDs studied. Nij requirements are not defined by the FAA but are instead established as a requirement for automotive occupant safety defined by National Highway Traffic Safety Administration (NHTSA) [15]. The Nij equation is the following, where F_{int} and M_{int} are intercept values specific to ATD configuration:

$$N_{ij} = \frac{F_z}{F_{int}} + \frac{M_y}{M_{int}} \qquad (2)$$

NHTSA requires an Nij value of less than 1.0 for automotive vehicle certification and a value of 1.0 corresponds with a 15% risk of severe injury to the cervical spine. All ATDs recorded Nij values under the established limits with the exception of the 95th ATD, which measured an Nij value of 3.36. The values are summarized in Table 2.

The high Nij value measured in the 95th ATD, indicates that the roof collapse did affect the ATD in this location. All other ATDs measured Nij values well below the 1.0 threshold.

Table 2 - ATD Nij values.

ATD	Nij Value
1 – HIII 10 YO - Front Stbd	Not Calculated
2 – HII 50th - Font Port	Not Calculated
3 – FAA HIII 50th - Middle Stbd	0.66
4 – FAA HIII 50th - Middle Port	0.33
5 – HIII 95th - Rear Stbd	3.36
6 – HIII 5th - Rear Port	0.73

The 95th ATD was out of family with the other values, so the values at the neck were plotted for further examination. The neck loads and moment are plotted in Figure 19.

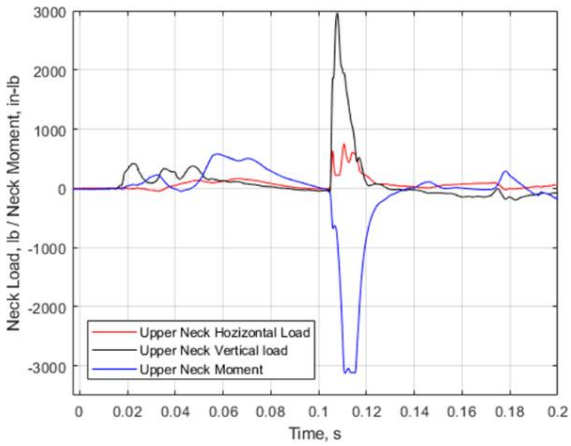

Figure 19 - HIII 95th upper neck loads and moment.

The data from the HIII 95th upper neck show a large event that occurred 110 ms after impact. The likely event that has occurred at this time is the overhead mass contacting the ATD head. The videos obtained are not able to confirm this event, however, the accelerations measured at the rear starboard mass location do show a spike at this time also.

FAA regulations require that lumbar loads from a 50th percentile HII or HIII FAA ATD not exceed 1,500 lb in 14 CFR 2X.562 [10-11]. The measured lumbar loads are shown in Table 3.

Table 3 - ATD lumbar load values.

ATD	**Lumbar Load (lb.)**
1 – HIII 10 YO - Front Stbd	862.4
2 – HII 50th - Font Port	1216.9
3 – FAA HIII 50th - Middle Stbd	2499.7
4 – FAA HIII 50th - Middle Port	1347.1
5 – HIII 95th - Rear Stbd	1864.7
6 – HIII 5th - Rear Port	2173.0

The two 50th percentile ATD's in energy absorbing seats (two & four), both indicated lumbar loads below the 1,500 lb injury metric limit. The 50th percentile ATD in the rigid seat three measured loads approximately 1,000 lb above the limit. These results indicate the importance of a seat stroking mechanism used in conjunction with energy absorbing capabilities of the aircraft structure to reduce occupant injury risk.

The effect of seat energy absorption was studied by comparing the adjacent HIII 50th FAA ATDs in the NASA EA (seat four) and rigid seat (seat three). The effect of the seat stroke and subfloor EA on ATD response was determined through comparison of these matching ATDs in the same row. An image series showing significant notable events during the EA seat stroking is shown in Figure 20. The NASA EA stroking seat is on the left while the rigid seat is on the right. The rigid seat images have been mirrored such that direct observations can be made.

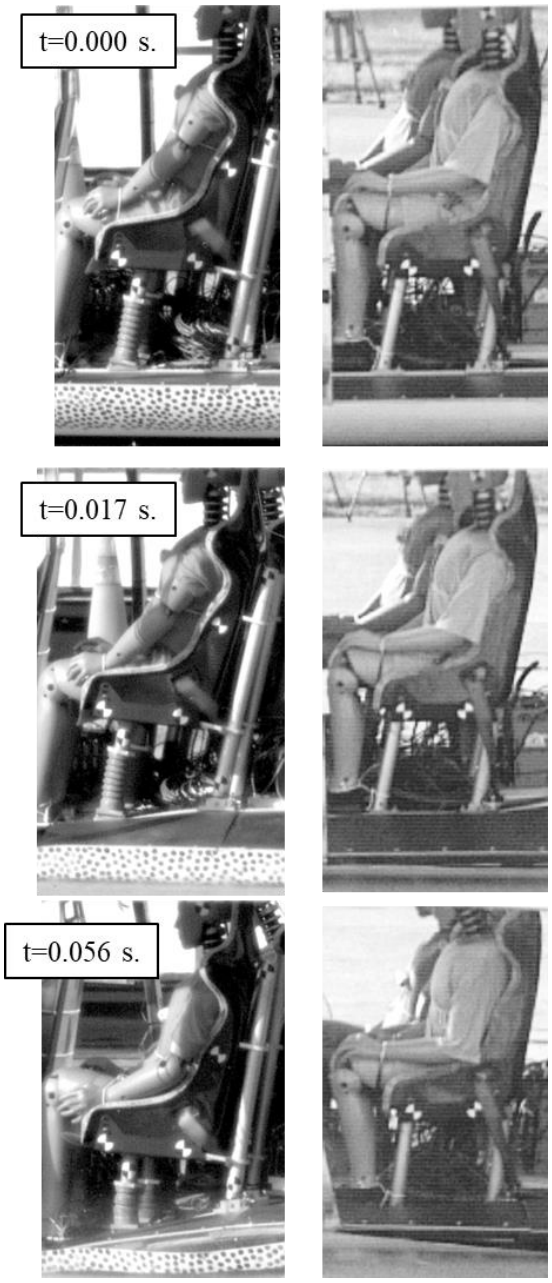

Figure 20 - NASA EA stroking (left) vs. rigid (right) seat responses.

The top set of images in Figure 20 show the ATDs seated in their respective seats at the time of ground impact. The second set of images show the ATDs in their seat after a large portion of subfloor EA cruciform stroke has completed and prior to the seat EA engaging. The bottom set of images show the ATDs after the seat stroke had occurred. It should be noted that up until the seat EA engaged, the responses looked largely the same. The seat stroke time history was captured and is shown in Figure 21. The stroking

data was obtained via photogrammetric techniques which were only able to resolve the first 100 ms of data after impact.

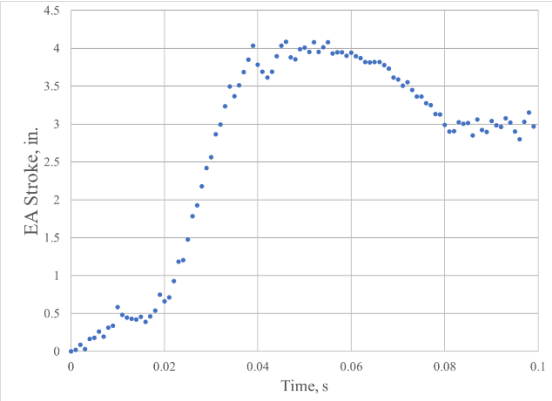

Figure 21 - Energy absorbing seat stroke displacement.

The stroking data presented in Figure 21 follows the trends seen in Figure 20. The stroke did not initiate until 17 ms after impact, and then continues for the next 30 ms after which a maximum stroke value of approximately 4 inches was achieved. There is a slight rebound in the seat/ATD after which the EA exhibited a permanent stroke of approximately 3 inches.

Lumbar load time histories are plotted and compared between the NASA EA and the rigid seat ATDs. The lumbar load time histories are shown in Figure 22.

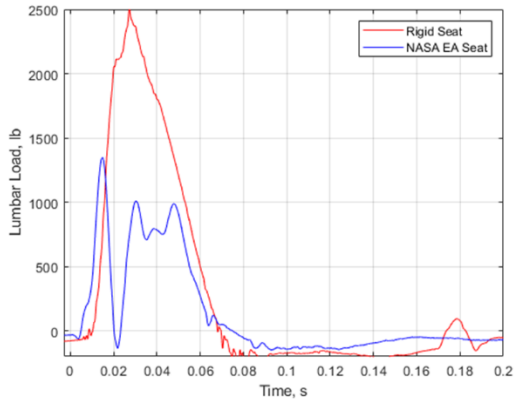

Figure 22 - Lumbar load comparisons between NASA EA and rigid seat.

During the first 17 ms of the impact, the ATD lumbar load values in the NASA EA and rigid seats were tracking approximately the same upward trends. The EA seat began to stroke at approximately 17 ms, and at this point the ATD experienced a dynamic unload due to the now downward motion of the seat. As the seat EA crushed the lumbar load profile of the ATD resembled a trapezoid at a plateau value of less than 1,000 lb. In contrast, the lumbar load values in the ATD in the rigid seat continued to increase to a peak of approximately 2,500 lb which occurred 28 ms after impact. The full duration of the load was defined as the duration from initial rise to the load crossing the y-axis, and determined as approximately 70 ms for both ATDs.

Lumbar loads from the 95th and 5th ATDs are also included in Table 3, even though these values are not used in the regulations. There is some documentation of lumbar load limits presented in a Full Spectrum Crashworthiness (FSC) Criteria for Rotorcraft [16] that discusses limits for non-standard sized ATDs such as the 5th (limit of 933 lb.) and 95th (limit of 1,757 lb.). Using those limits, a normalized lumbar load plot is shown in Figure 23.

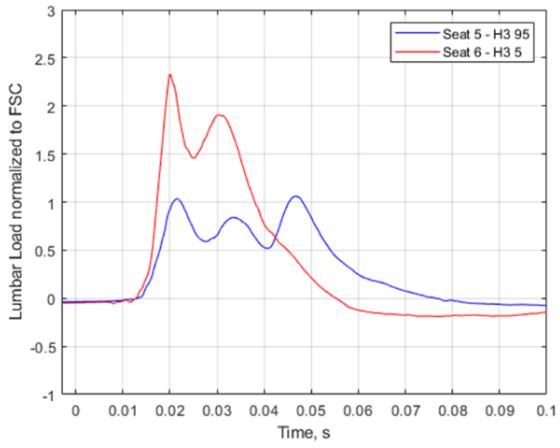

Figure 23 - Normalized lumbar load values of the 5th and 95th ATDs.

Perhaps counterintuitively, the 95th ATD data showed a lower normalized value, only very slightly above the limit value at 1.1, whereas the 5th sized ATD normalized lumbar load value was significantly higher at 2.3. However, further investigations into the subfloor structure revealed the source behind this behavior. By examining the post-test shapes of the cruciforms that were located under these two ATDs, it was found that that cruciform subfloor under the 95th ATD crushed more efficiently than for the 5th. The finding is supported by examining the shape of the plots in Figure 23. The 95th ATD has a lower overall peak value and is trapezoidal shaped with a defined

region approximating a plateau. This region of sustained lumbar load was largely below the threshold with only a slight overage during the onset and toward the end of the response. The 5th ATD data, in contrast, was of much shorter duration and higher in magnitude, suggesting less crushing of the cruciform. While the 5th ATD lumbar load data did exhibit a slightly trapezoidal pulse, the EA subfloor was not efficient enough to keep the lumbar load values below the normalized limits. While it was difficult to determine the maximum amount of crush of the subfloor cruciform during the test since there were no measuring devices on the cruciforms themselves, the cruciforms were measured post-test after being extracted from the test article. The cruciform underneath the 5th ATD experienced a permanent post-test crush depth of between ½ inch and 1 inch. In contrast, the cruciform underneath the 95th percentile ATD experienced a post-test permanent crush depth of between 1 inch and 2 inches. A picture of the two EA cruciforms in the test article, prior to extraction, are shown in Figure 24.

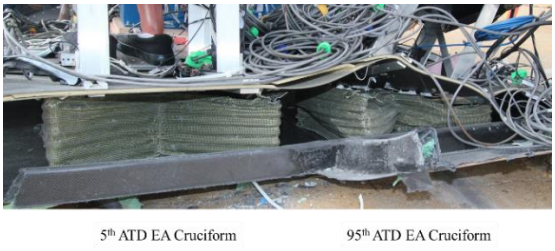

Figure 24 - EA cruciforms for the 5th and 95th ATDs.

The post-test EA cruciforms, still installed in the test article but with all other structure removed, are shown in Figure 25.

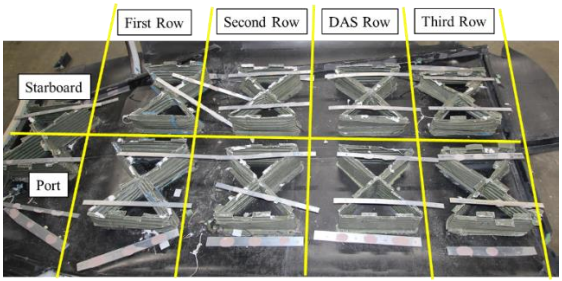

Figure 25 - Subfloor EA cruciforms post-test.

Post-test examinations of the tested EA cruciforms revealed several notable items. The first was the EAs themselves, while in various states of crush, did not show signs of buckling or collapse, indicating robustness toward the longitudinal forces induced from the forward deceleration of the test article at impact. The second was that there was indication of crush on all specimens, indicating that they did accomplish their required goal of absorbing impact energy of the test. The post-test measured delta lengths of the specimen, as measured in the middle of and the edges of each specimen, are shown in Table 4. Note these values do not represent the maximum crush experienced during the test, but rather a permanently deformed condition extracted from the test article post-test. It is intended to give a relative measure for comparative purposes and will be used in additional post-test inspections and for further EA optimization.

Table 4 - EA subfloor post-test crush.

Cruciform Location	**Middle post-test crush delta (inch)**	**Edge post-test crush delta (inch)**
First Row - Port	0.5	0.5
First Row – Stbd	0.5	0.5 - 1.0
Second row – Port	0.5	0.5
Second Row – Stbd	0.5	0 - 0.5
DAS Row – Port	1.0	0.5
DAS Row - Stbd	0.0	0.0
Third Row – Port	1.0	1.5
Third Row - Stbd	2.0	1.0

SUMMARY

In late 2022, a full-scale crash test was conducted at NASA LaRC on an eVTOL Lift Plus Cruise concept design. The purpose of the test was to generate data to be used in the development of consensus standards, to evaluate a variety of energy absorbing concepts, to assess injury on a variety of sized ATD onboard occupants, and to validate computational modelling efforts.

The test article development process was conducted primarily through the use of computational simulations. The simulations were used to size various components, determine material properties, develop the energy absorbing mechanisms, and to identify relevant impact conditions. The test produced events both predicted and not predicted within the pre-test vehicle simulations.

The main two events that occurred during the test were the crushing of the subfloor and seat energy absorbing structure and the collapse of the roof due to the presence of the overhead mass. The energy absorbing mechanism crushing occurred during the first the two events. The energy absorbing subfloors began to crush immediately upon impact and crushed to varying levels of stroke. While it was impossible to measure the amount of stroke that occurred on the structures during the test, the cruciforms post-impact shapes were documented during post-test teardown of the test article.

Roof collapse begin with the vertical stiffeners began to fail approximately 36 ms after impact. Failures of the a-,b- and c-pillars on the starboard side and the b-, and c-pillars on the ports side led to large amounts of compression and vertical motion at the aft end of the cabin section. The collapse occurred between the initial failures at 36 ms to approximately 200 ms after impact.

The calculated lumbar load values for the ATDs seated in the energy absorbing seats were below established FAA certification limits. The 50th FAA HIII sitting in the rigid seat was above the established limits. The 95th and 5th ATDs were over the FSC criteria limits, with the 95th ATD only briefly exceeding this limit.

ATD HIC36 limits were below the established criteria for all ATDs examined. In the case of the 95th ATD, data dropout prohibited the computation of the HIC36 value. Nij limits were below established limits for all ATDs computed with the exception of the 95th ATD. This ATD had Nij values over the established limits, which gives indication there was some effect of the roof collapse on the ATD in this location.

DISCUSSION

The crash test performed on the NASA eVTOL LPC design provided data demonstrating capabilities of energy absorbing structures to improve crashworthiness and information on full-scale composite aircraft structural response to dynamic impact conditions. The data will help guide future NASA efforts for modelling and simulation, along with further refinement of the energy absorbing mechanisms used.

Additional consideration should be given to the optimization of the subfloor structures. When examining the data, it appeared that the subfloors were most efficient for the heavier occupants such as the 95th ATD. While the subfloors did crush under all of the occupants during the test to varying degrees, the amount of loading into the occupant was most limited in the 95th ATD. In addition, the loads will be most reduced when an energy absorbing subfloor and energy absorbing seat work together as a system. NASA will continue to optimize the EA components both in the subfloors and in the seats using the results from this test to further reduce injury risk for the onboard occupants.

The roof collapse, leading to the intrusion of the overhead mass, likely affected the rear row and specifically the 95th ATD, which showed high values of neck loads. The results obtained showed items that were not predicted from pre-test predictions, but nonetheless provide valuable insight into the nature of failure modes, energy absorbing structures and occupant response.

NASA is currently in the middle of fabricating and plans on testing a second LPC test article. The information gathered from the test described in this report along with updated computational modelling predictions will be used to define parameters for the second test. Additional factors such as assumptions on overhead mass, seat design, and occupant sizes are additional items that will be considered prior to the second test.

Testing by NASA on a composite eVTOL concept vehicle is intended to be utilized by the eVTOL community such that insight can be gained into computational simulation response, energy absorbing development, and of composite airframe structural response in representative loading environments. Additionally, by conducting tests prior to widespread eVTOL operations, the data could be used to guide further development, or aid in the advancement toward widespread market adoption.

REFERENCES

1. Krishnamurthy, S. et al. “Prediction-Based Auralization of a Multirotor Urban Air Mobility Vehicle.” Proceedings from the

2021 AIAA SciTech Forum. Virtual. Jan 11-21, 2021.
2. Simmons, B.M. "Efficient Variable-Pitch Propeller Aerodynamic Model Development for Vectored-Thrust Aircraft." Proceedings from the AIAA Aviation Conference. Chicago IL. June 27 – July 1, 2022.
3. Edwards, T. et al. "Exploring Human Factors Issues for Urban Air Mobility Operations." AIAA Aviation and Aeronautics Forum. Dallas TX. June 17-21, 2019.
4. Putnam, J.B., and Littell, J.D. "Evaluation of Impact Energy Attenuators and Composite Material Designs of a UAM VTOL Concept Vehicle." Proceedings from the Vertical Flight Society 75th Annual Forum and Technology Display. Philadelphia PA. May 13-16, 2019.
5. Silva, C., Johnson, W., Antcliff, K.R., and Patterson, M.D. "VTOL Urban Air mobility Concept Vehicles for Technology Development." Proceedings from the 2018 Aviation Technology, Integration, and Operations Conference, June 25-29, 2018, Atlanta GA.
6. Littell, J.D., Putnam, J.B., and Cooper, M. "Simulation of Lift plus Cruise Vehicle Models to Define a Full-Scale Crash Test Campaign." Proceedings from the Vertical Flight Society 77th Annual Forum and Technology Display. Virtual. May 10-14, 2021.
7. Federal Aviation Administration. "General." 14 CFR § 27.561. Amended March 13, 1996.
8. Littell, J.D., et al. "The Evaluation of Composite Energy Absorbers for use in UAM eVTOL Vehicle Impact Attenuation." Proceedings from the Vertical Flight Society 75th Annual Forum and Technology Display. Philadelphia PA. May 13-16, 2019.
9. Putnam, J.B., et al. "Development and Analysis of Energy Absorbing Subfloor Concepts to Improve eVTOL Crashworthiness." Proceedings from the Vertical Flight Society 78th Annual Forum. Ft. Worth TX. May 10-12, 2022.
10. Federal Aviation Administration. "Emergency Landing Dynamic Conditions." 14 CFR § 23.562. Amended February 9, 1996.
11. Federal Aviation Administration. "Emergency Landing Dynamic Conditions." 14 CFR § 27.562. Amended November 13, 1989.
12. Kellas, S., et al. "Full Scale Crash test of an MD-500 Helicopter with Deployable Energy Absorbers." Proceedings from the American Helicopter Society 66th Annual Forum. Phoenix AZ. May 11-13, 2010.
13. Society of Automotive Engineers (SAE). "Surface Vehicle Recommended Practice: Instrumentation for Impact Test-Part 1-Electronic Instrumentation." SAE J211-1. 2007.
14. Kleinberger, M., Sun, E., Eppinger, R., Kuppa, S., and Saul, R. "Development of Improved Injury Criteria for the Assessment of Advanced Automotive Restraint Systems." National Highway Traffic Safety Administration, Washington, DC, 1998.
15. National Highway Traffic Safety Administration. "Occupant Crash Protection." 49 CFR § 571.208. September 26, 2022.
16. Bolukbasi, A., et al. "Full Spectrum Crashworthiness Criteria for Rotorcraft." RDECOM TR 12-D-12. December 2011.